diffusion-fundamentals.org
The Open-Access Journal for the Basic Principles of Diffusion Theory, Experiment and Application

Reconstructing undersampled MR Images by utilizing principal-component-analysis-based pattern recognition

Fangrong Zong,[1] *Marcel Nogueira d'Eurydice*,[1] *Petrik Galvosas*[1]

[1]MacDiarmid Institute for Advanced Materials and Nanotechnology,Victoria University of Wellington, Wellington, New Zealand

Corresponding author: Petrik Galvosas, MacDiarmid Institute for Advanced Materials and Nanotechnology, School of Chemical and Physical Sciences, Victoria University of Wellington, PO Box 600, Wellington 6140, New Zealand. E-mail: Petrik.Galvosas@vuw.ac.nz.

Abstract

Compressed sensing technique is a recent framework for signal sampling and recovery. It allows signal acquisition with less sampling than required by Nyquist-Shannon theorem and reduces data acquisition time in MRI. When the sampling rate is low, prior knowledge is essential to reconstruct the missing features. In this paper, a different reconstruction method is proposed by using the principal component analysis based on pattern recognition. The experiments demonstrate that this method can reduce aliasing artefacts and achieve a high peak signal-to-noise ratio compared to a compressed sensing reconstruction.

Keywords:

MRI; Fast imaging; Principal components analysis; Recognition; Compressed sensing;

1 Introduction

Acquisition of MRI in clinical applications may be time-consuming and may lead to reduced patient throughputs and increased image artefacts due to the patient moving during imaging. Reducing imaging time is financially beneficial to a total cost and can facilitate more studies as well. One approach of speeding up the acquisition of MRI is to undersample *k*-space data. Aliasing artefacts due to the violation of Nyquist-Shannon rule [1, 2] in the reconstructed magnetic resonance (MR) images can be reduced by a randomly undersampling format [3, 4], which is part of the Compressed Sensing (CS) framework. CS techniques have been extensively used in undersampled MRI reconstruction since 2006 [5–8]. The premise of applying a CS framework is that the MR images are sparse in a certain orthogonal transformation domain (aka basis) [5, 9]. However, when the object is largely undersampled, the missing features may not be satisfyingly reconstructed. In this situation, prior knowledge of similar images can provide constructive information to recover those features, such as shapes and relative contrast to the surrounding tissues.

Principal component analysis (PCA) is a useful statistical technique that extracting the principal components from a set of objects (similar images, in our case) [10, 11]. The number of principal components is less than or equal to the number of images in the database, thus the combination of

principal components from PCA can be used as a transformation domain in the CS reconstruction. This has been proved effective for the recovery of the signal from undersampled data in wireless sensor networks [12], or the extraction of NMR parameter mappings based on k-t data (e.g. [7]) and will be referred as PCA-CS hereafter.

In this paper, PCA recognition reconstruction (PCA-RR) is proposed to improve the MR image quality, by utilising PCA based on pattern recognition. This method is different from the CS reconstruction but shares many of its benefits. Instead of enforcing one matched image as a sparse representation, a subset of the MR images are chosen to complement the undersampled *k*-space data of the image under study. Peak-Signal-to-Noise-Ratio (PSNR) [13] is calculated to evaluate and compare the performance of PCA-RR and PCA-CS at two different sampling rates.

2 Materials and method

2.1 Phantom and sampling information

As approachable biological samples, carrots were chosen to verify the feasibility of the proposed algorithms. Twenty-five carrot taproots were used to obtain 200 axial images in total. MRI data was acquired on a 9.4 T Bruker BioSpec pre-clinical MRI system using the multi-slice spin echo pulse sequence with the repetition time of 6 s and echo time of 15 ms. The slices of the MR images have a thickness of 2 mm with an interval of 4 mm. The field of view is 25×25 mm^2 with the resolution of 0.0977×0.0977 mm^2. Thus, each slice has a data-size of 256×256.

The full *k*-space data was acquired by the MRI system and random masks were designed in order to obtain the undersampled *k*-space data of certain slices. The schematic of the undersampling mask with sampling rates of 20% and 50% for the *k*-space data is shown in Fig.1. The white areas mean that the corresponding *k*-space data was sampled, whilst the *k*-space data in the black areas was filled with zeros. These undersampling masks are based on the Cartesian coordinates. When the sampling rate is 50%, it means that 128 (=256×0.5) random lines in the phase direction are used for future processing; when the sampling rate is 20%, only 51 random lines are used, which lose more information than 50% sampling. All algorithms were implemented on Matlab (The Mathworks, Natick, MA).

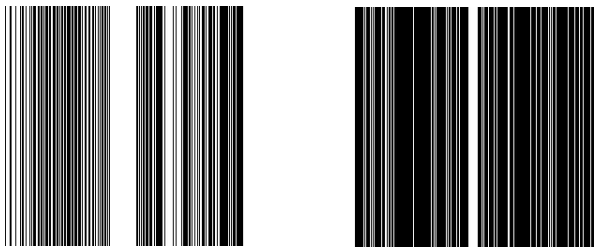

(a) (b)

Fig. 1: Random undersampled masks, sampling rate is (a) 0.5; (b) 0.2.

2.2 Reconstruction procedure using PCA (PCA-RR)

The determination of the principal component basis and the procedure of the principal components analysis are illustrated in the dashed box of Fig. 2. Before performing the PCA procedure, each image in the database ($\mathbf{I}_1,...\mathbf{I}_d$) is re-arranged to a vector ($\vec{I}_1,...\vec{I}_d$), thus the database can be treated as a matrix ($\mathbf{D}$) with the row size equal to the number of pixels ($M\times N$) in one image and the column size of d (the number of images in the database). A covariance matrix ($\mathbf{G}$) is constructed using the database matrix $\mathbf{D}$:

$$\mathbf{G} = (\mathbf{D}-\mathbf{M})^T(\mathbf{D}-\mathbf{M}) \tag{1}$$

where $\mathbf{M}$ is the mean matrix, and the columns in $\mathbf{M}$ are identical, which are equal to the mean vector from ($\vec{I}_1,...\vec{I}_d$). As a result, the elements in the covariance matrix indicate the correlation of the image vectors in the database. By performing the eigen-decomposition of $\mathbf{G}$, the eigenvectors and eigen-

values can be determined. $\mathbf{B} = (\mathbf{b}_1, ..., \mathbf{b}_i, \mathbf{b}_n)$, $\mathbf{b}_i$ is the eigenvectors, which can produce *principal components* in PCA. Then, each image has the unique projection coefficients ($\mathbf{PJ}_i$) by projecting the image to the principal components, no matter it is in the database or not. This means that we can use projection coefficients and principal components to fully or approximately reconstructed images. Here, we propose a method called PCA recognition reconstruction (PCA-RR), and the procedure is outlined as Fig. 2.

In Fig. 2, a vector of projection ($\mathbf{PJ}'$) is obtained from projecting the undersampled image to the principal components. A subset of q images in the database are selected when their Euclidean distance (d_{ei}) between the corresponding $\mathbf{PJ}$ and $\mathbf{PJ}'$ is smaller than δ, which is a user-controlling parameter sensitively determining the performance of the algorithm. The detailed discussion of choosing δ is beyond the text. Subsequently, these q images are used to constitute an image $\mathbf{I}_c$ with the corresponding weighting factor, i.e. the inverse of the normalized Euclidean distance. After that, the estimated k-space data via Fourier Transform (FT) was used to fill the missing k-space. In other words, the measured k-space data was kept during the iteration procedure, the unmeasured k-space data was filled with different estimated data until the images of the neighbouring iterations satisfy the condition:

$$||\mathbf{I}_u(p) - \mathbf{I}_u(p-1)||_2 < \varepsilon \tag{2}$$

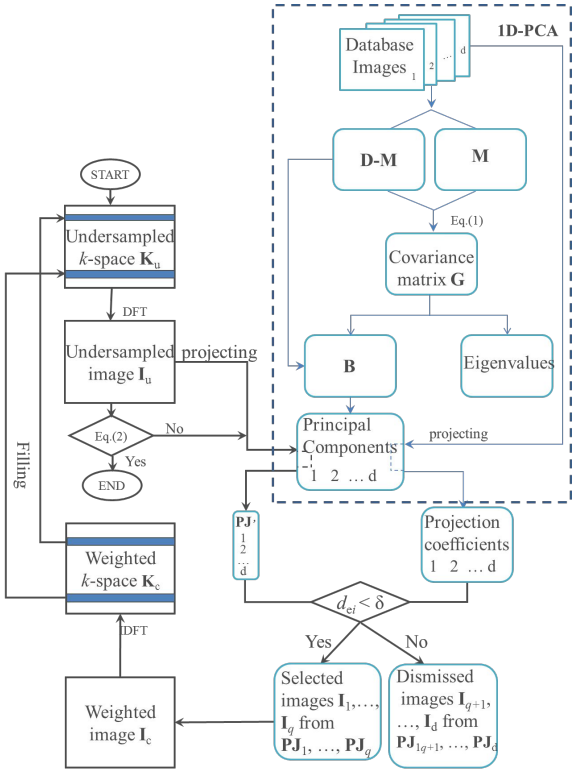

Fig. 2: The flow chart of the PCA-RR procedure.

3 Results and discussion

The reconstructed data was quantitatively evaluated in terms of PSNR. PSNR measures the differences between the reconstructed image and the original image, and is defined by[13]

$$\mathrm{PSNR} = 20\log_{10}\left(\frac{\mathrm{MAX}}{\sqrt{\mathrm{MSE}}}\right) \tag{3}$$

where, MSE is the mean square error and MAX is the maximum pixel value of the image.

The reconstructed results of an undersampled image with 50% sampling rate is shown in Fig. 3. The full k-space information was excluded from the database. Since the sampling rate was moder-

ate, the undersampled image via zero-filling FT still preserved much of the information (Fig. 3(a)). Fig. 3(b) is the reconstructed results using PCA-CS, keeping 174 principal components (with the corresponding projection coefficients larger than 5e-3). Fig. 3 (b) and (c) are the reconstructed results using PCA-CS (keeping 174 principal components) and PCA-RR (choosing 6 matched images), respectively. PSNR of PCA-RR, PCA-CS and zero-filling FT are identical within uncertainties.

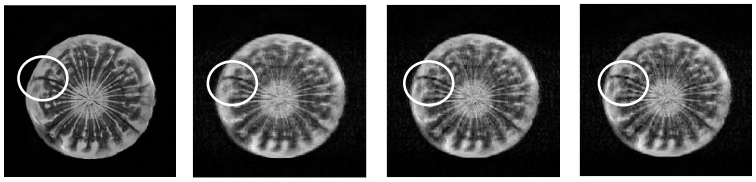

(a) (b) (c) (d)

Fig. 3: Reconstruction results of the undersampled image with sampling rate is 0.5: (a) the full image; (b) the undersampled image via zero-filling FT (PSNR = 24.654); (c) reconstructed images using PCA-CS method (PSNR = 24.679); (d) reconstructed images from PCA-RR (PSNR = 24.696)

The reconstructed results of the same image (Fig. 3(a)) with 20% sampling rate is shown in Fig. 4. Due to the high undersampling rate, the undersampled image via zero-filling FT had more blurring and a smaller PSNR (Fig. 4(b)) compared with Fig. 3(b). Fig. 3(c) is the reconstructed results using PCA-CS, with the same threshold of the projection coefficients (5e-3) as described above. The number of principal components used here was smaller than 50% sampling. PCA-CS filled more details in the centre and reduced the blurring compared to the undersampled image. The feature in the white circle in Fig. 4(b) was suppressed after using PCA-CS reconstruction. Fig. 4(c) is the reconstructed results using PCA-RR, by choosing 6 matched images. Like the PCA-CS results, more details and less blurring in PCA-RR can be seen, but the difference from PCA-CS is that the white circled feature can be clearly reconstructed. Moreover, the PSNR of the reconstructed images via PCA-RR is higher than zero-filling FT and PCA-CS.

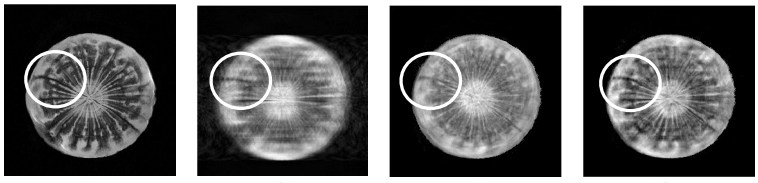

(a) (b) (c) (d)

Fig. 4: Reconstruction results of the undersampled image with sampling rate is 0.2: (a) the full image; (b) the undersampled image via zero-filling FT (PSNR = 17.520); (c) the reconstructed image using PCA-CS (PSNR = 19.887); (d) the reconstructed image from PCA-RR (PSNR = 17.978)

The number of iterations were compared when the sampling rate was 50% and 20% and are illustrated in Fig. 5. The number of iterations is larger than 7 when the sampling rate is 20%, whilst this value decreased to less than 4 when the sampling rate was 50%. As can be seen from Fig. 5, more iterations was needed when the sampling rate was lower.

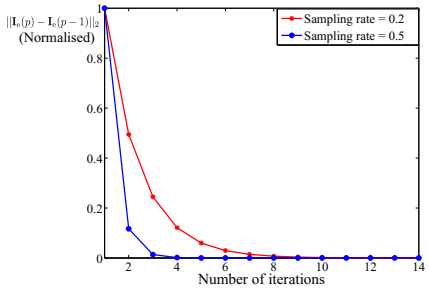

Fig. 5: Comparison of the number of iterations with different sampling rates

4 Conclusions

A new reconstruction method (PCA-RR) for highly undersampled MR images was proposed in this paper. When the *k*-space data is highly undersampled, it is important to draw on prior knowledge of the sample during the reconstruction. PCA-RR utilises the merits of a PCA-based pattern recognition procedure. In the meantime, it shares the benefits of reduced acquisition time as typical for CS schemes, filling the unsampled *k*-space data with an iterated procedure. The experimental results of two undersampled carrot images with different sampling rates were shown in this paper. The undersampled image via zero-filling FT can preserve more information when sampling at a higher rate. Furthermore, when the sampling rate is lower, more iterations are required to obtain the same result as with the higher sampling rate. Nevertheless, in both cases, the PSNR of PCA-RR is higher than PCA-CS, which demonstrated that PCA-RR was valid and superior to PCA-CS.

5 Acknowledgements

The work was supported by the New Zealand Ministry of Business, Innovation, and Employment via the Grant "New NMR Technologies". The authors would like to thank Dr. Paul Teal for useful discussions on the mathematics of CS scheme. The authors would also like to thank Mr.Phillip Luey for language help and proof reading the manuscript.

References

[1] H. Nyquist, Certain topics in telegraph transmission theory, Trans. AIEE 47 (2) (1928) 617–644.
[2] C. E. Shannon, Communication in the presence of noise, Proc. Institute of Radio Engineers 37 (1) (1949) 10–21.
[3] E. Candès, J. Romberg, Sparsity and incoherence in compressive sampling, Inverse Probl 23 (3) (2007) 969.
[4] E. Candès, M. Wakin, An introduction to compressive sampling, IEEE Signal Process Mag 25 (2) (2008) 21–30.
[5] M. Lustig, D. Donoho, J. Pauly, Sparse mri: The application of compressed sensing for rapid mr imaging, Magn Reson Med 58 (6) (2007) 1182–1195.
[6] T. Wech, A. Lemke, D. Medway, L.-A. Stork, C. A. Lygate, S. Neubauer, H. Köstler, J. E. Schneider, Accelerating cine-MR imaging in mouse hearts using compressed sensing., J. Magn. Reson. Imaging 34 (5) (2011) 1072–1079.
[7] C. Huang, C. G. Graff, E. W. Clarkson, A. Bilgin, M. I. Altbach, T_2 mapping from highly undersampled data by reconstruction of principal component coefficient maps using compressed sensing., Magn. Reson. Med. 67 (5) (2012) 1355–1366.
[8] P. W. Worters, K. Sung, K. J. Stevens, K. M. Koch, B. a. Hargreaves, Compressed-sensing multispectral imaging of the postoperative spine., J. Magn. Reson. Imaging 37 (1) (2013) 243–248.
[9] X. Qu, W. Zhang, D. Guo, C. Cai, S. Cai, Z. Chen, Iterative thresholding compressed sensing mri based on contourlet transform, Inverse Problems in Science and Engineering 18 (6) (2010) 737–758.
[10] M. Turk, A. Pentland, Eigenfaces for recognition, J Cognit Neurosci 3 (1) (1991) 71–86.
[11] L. I. Smith, A tutorial on Principal Components Analysis Introduction, Cornell Univ. USA 51 (2002) 1–26.
[12] R. Masiero, G. Quer, D. Munaretto, M. Rossi, J. Widmer, M. Zorzi, Data acquisition through joint compressive sensing and principal component analysis, in: Proceedings of the 28th IEEE on Global Telecommunications Conference., IEEE, 2009, pp. 1–6.
[13] A. Eskicioglu, P. Fisher, Image quality measures and their performance, IEEE Trans Comm 43 (12) (1995) 2959–2965.